Authors' version of a paper published in
"IEEE Sensors Letters"

Paper reference: K. Abbas, P. Chatelain, M. Puigt, G. Delmaire and G. Roussel, "Fabry-Perot Spectral Deconvolution with Entropy-weighted Penalization," in IEEE Sensors Letters, vol. 8, no. 9, pp. 1-4, Sept. 2024.

IEEE online version: `https://dx.doi.org/10.1109/LSENS.2024.3439209`.

Copyright: ©2024 IEEE. Personal use of this material is permitted. Permission from IEEE must be obtained for all other uses, including reprinting/republishing this material for advertising or promotional purposes, collecting new collected works for resale or redistribution to servers or lists, or reuse of any copyrighted component of this work in other works.

Sensor Applications

Fabry-Perot Spectral Deconvolution with Entropy-weighted Penalization

Kinan Abbas[1*], Pierre Chatelain[1], Matthieu Puigt[1**], Gilles Delmaire[1], and Gilles Roussel[1]

[1] *Univ. Littoral Côte d'Opale, LISIC – UR 4491, F-62219 Longuenesse, France*
[*] *Student Member, IEEE*
[**] *Member, IEEE*

Abstract—Miniaturized CMOS hyperspectral cameras utilizing Fabry-Perot Interferometers (FPIs) have emerged as a low-cost solution providing fast-acquisition miniaturized sensors well-suited for both in-field analysis and remote sensing. However, FPIs generate harmonics around each wavelength of interest, hindering the accuracy and reliability of spectral information. This paper proposes a novel scene-dependent spectral correction and calibration method for miniaturized CMOS hyperspectral cameras using FPI technology. Unlike the manufacturer's scene-independent spectral correction matrix, our approach utilizes deconvolution with Tikhonov regularization weighted by the entropy of the Fabry-Perot harmonics to remove the generated artifacts and restore the original spectra. It adapts to the scene's unique characteristics, reducing harmonics and improving hyperspectral data quality. The experiments on synthetic data and real images acquired by an FPI sensor demonstrate the superiority of our method in removing harmonic distortions and achieving improved accuracy in spectral calibration.

Index Terms—Sensor signal processing, Hyperspectral Imaging, CMOS sensors, Fabry-Perot, Calibration, Spectral Correction.

I. INTRODUCTION

Hyperspectral imaging (HSI) is a powerful tool that captures a scene spectral reflectance at multiple wavelengths enabling applications in various fields [1]. Traditional hyperspectral cameras have significant drawbacks, such as high cost, bulky size, and limited spatial resolution, making them less suitable for applications that require mobility and rapid data acquisition [2]. Therefore, miniaturized CMOS hyperspectral cameras based on Fabry-Perot interferometer (FPI) have emerged as a low-cost, fast-acquisition, and portable solution for HSI [3]–[5]. FPI is a widely used tool for spectral filtering in optical systems. Spectral cameras using FPIs have been developed by integrating them monolithically on top of CMOS image sensors. The filter's cavity length and mirror reflectivity determine the selected wavelength and spectral bandwidth respectively. In addition, using CMOS process technology reduces cost and improves the compactness of hyperspectral cameras. Thus, enabling multiple applications in agriculture, autonomous driving, and surveillance.

The filter layout describes the pattern in which the filters are deposited on the sensor, and currently, major designs are *Linescan Wedge* and *Snapshot Mosaic*. There are variations for each layout, depending on the type, the active range of the sensor and the number of different filters in the layout [6]. Ideally, an FPI would efficiently transmit light within a narrow spectral range to the sensor while blocking light outside this range. However, FPIs exhibit additional harmonic responses around each desired wavelength in practical implementations. Moreover, CMOS cameras encounter various impurities, such as spectral leaking, spectral shifting, cross-talk in the snapshot mosaic cameras [7]. These issues were solved by the camera manufacturer. Specifically, it proposes a scene-independent spectral correction matrix to suppress the FPI second-order harmonics. This method, however, is not always practical, as it does not consider the unique characteristics of the observed scene. Furthermore, we proposed in [8] an accurate endmember estimation technique which deconvolves FPI "pure patches". As it is working on raw data, the above spectral correction matrix cannot be applied.

This paper presents our novel contribution to the field, a scene-dependent spectral correction and calibration method for miniaturized CMOS hyperspectral cameras using FPI technology. By leveraging the deconvolution of the sensor response matrix with entropy-weighted Tikhonov regularization, our approach effectively suppresses harmonics and cross-talk and enhances the quality of hyperspectral data. It is worth noting that spectral reconstruction encompasses various applications, i.e., spectral reconstruction from a limited set of measurements [9]. Our main contribution focuses on spectral correction, which involves converting raw digital numbers (DN) from imaging sensors into physical quantities like reflectance or radiance [10]. Experiments with synthetic data and real images from both linescan wedge and snapshot mosaic IMEC sensors show our method outperforms the manufacturer solution in eliminating harmonics and enhancing spectral information.

The remainder of the paper is organized as follows: Section II discusses image processing and spectral correction. Our method is introduced in Section III, evaluated in Section IV, with conclusions and future work in Section V.

II. RELATED WORK

Spectral cameras using FPIs have been developed by monolithically integrating them on top of CMOS image sensors resulting in two major designs used in commercially available cameras, i.e., *Linescan Wedge* [5] and *Snapshot Mosaic* [3]. The linescan wedge design segments the sensor into k bandlets, each a unique FPI capturing varied spectral scene data arranged in an increasing cavity height, forming a discrete wedge. To create the full datacube, raw images need to be stitched together and aligned. [4]. The snapshot mosaic arranges filters per pixel within a $\sqrt{k} \times \sqrt{k}$ cell, extending the FPI for full sensor rage [3]. A post-processing technique called "demosaicing" is required to estimate the complete hyperspectral data cube [11], [12].

An FPI efficiently transmits light within a specific spectral range to the sensor and blocks other light. However, FPIs also have additional harmonic responses at desired wavelengths. Cameras face challenges like spectral leakage, shifting, and CMOS imager performance

Corresponding author: K. Abbas (e-mail: kinan.3bbas@gmail.com).
Associate Editor: Alan Smithee.
Digital Object Identifier 10.1109/LSENS.2023.0000000

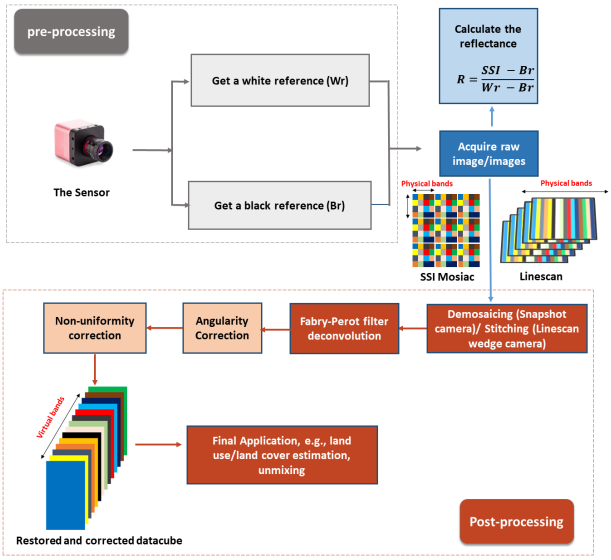

Fig. 1. Image processing pipeline for snapshot spectral and linescan cameras (Single Image Demosaicing vs. Multi-Image Stitching).

variations, necessitating pre-processing and post-processing for high-quality images [6], [7]. First, a rejection filter conditions the incident light, blocking wavelengths outside the sensor's active range to prevent spectral leakage and second-order responses [6]. Then, *dark level correction* (bias correction) is applied by subtracting a "dark image" from the raw image to remove sensor noise and offset, with this reference image captured with the lens closed. While the rejection filters remove most undesired wavelengths, some persist within the sensor active range, thus requiring *spectral correction*. The latter is performed by applying a fixed—i.e., scene-independent—correction matrix denoted $\mathbf{C}$ which is determined through a process of minimizing the difference between the actual band response, denoted as the response matrix $\mathbf{H}$, and the desired or ideal band response, represented as $\mathbf{H}^{\text{ideal}}$. This minimization process is expressed mathematically as [13]

$$\min_{\mathbf{C}} \|\mathbf{H}^{\text{ideal}} - \mathbf{C} \cdot \mathbf{H}\|_{\mathbb{F}}^2, \tag{1}$$

where $\|\cdot\|_{\mathbb{F}}^2$ denotes the Frobenius norm. To effectively apply this correction matrix, it typically requires the calculation of reflectance using a white reference [6]. The correction matrix $\mathbf{C}$ serves to transform physical wavelengths—as captured by the camera sensor—into virtual wavelengths, representing the spectrally-corrected data. The number of virtual bands is often less than that of the physical bands. Such discrepancies may arise from strong correlations among the responses of specific physical bands or from a lack of signal captured by one or more physical bands [6]. Furthermore, we note that the response matrix $\mathbf{H}$, which forms the foundation of our proposed framework, has crucial information about filter characteristics—including first and second-order responses—and the full width of response peaks at half the maximum of the peak (FWHM). By multiplying this matrix with an irradiance spectrum, we simulate the sensor response, thereby facilitating evaluations under realistic conditions. *Angularity correction* [14] adjusts for light angle variability, while *non-uniformity correction* addresses sensor discrepancies. Fig. 1 shows the processing pipeline of the images with the steps mentioned above.

Beyond the physical design and correction challenges of compact spectral cameras, entropy allows to quantify the level of information in a given system. Consider a d-dimensional probability vector, denoted as $\mathbf{p} = (p_1, p_2, \ldots, p_d)^T$ where each p_i represents the probability of the i^{th} event occurring in a d-dimensional probability space. The entropy of the vector $\mathbf{p}$ is defined as:

$$E(\mathbf{p}) = -\sum_{i}^{d} p_i \cdot \log(p_i). \tag{2}$$

The entropy here quantifies the uncertainty in $\mathbf{p}$'s values, peaking when $\mathbf{p}$'s distribution is consistent across all events and minimizing when one event dominates with near certainty [15].

Given the harmonics of the FPI shown in Fig. 2, the entropy of FPI harmonics is high with multiple peaks in the band response and near zero with a single peak. Incorporating this information into the deconvolution problem allows us to effectively control the level of smoothness required for the corrected spectrum.

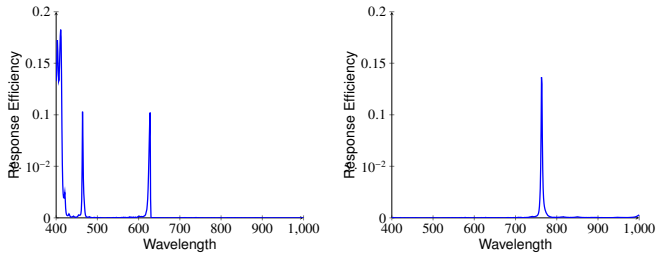

(a) Entropy = 0.54 (b) Entropy = 0.04

Fig. 2. Fabry-Perot filter responses for different bands of the linescan camera. On the left: 805 nm. On the right: 650 nm.

III. PROPOSED SPECTRAL CORRECTION METHOD

In our spectral imaging context, after the process of demosaicing or stitching, we encounter a datacube where each spatial pixel is a $k \times 1$ vector $\mathbf{z}$ with k representing the number of wavelengths, i.e.,

$$\mathbf{z} = \mathbf{H} \cdot \mathbf{x}. \tag{3}$$

Here, $\mathbf{H}$ is the response matrix with dimensions $k \times q$ where q is the number of measurement points used during the calibration of the sensor and $\mathbf{x}$ is the original spectrum that we intend to see in each pixel. In practice, $q = 601$ as the manufacturer samples responses at every 1 nm interval within the range of 400–1000 nm. The primary challenge we encounter is the estimation of the vector $\mathbf{x}$ based on the observed spectral pixel vector $\mathbf{z}$ and the response matrix $\mathbf{H}$. However, due to the available dimensions, estimating $\mathbf{x}$ is an under-determined problem. Additionally, the use of the cut-off filter results in the blocking of harmonics outside the sensor's active range, making the matrix $\mathbf{H}$ not suitable for the retrieval process. To address this, we propose to reduce the size of the matrix $\mathbf{H}$ to retain only the applicable information. This reduction is achieved through a strategic sampling of the matrix $\mathbf{H}$, keeping values corresponding to virtual wavelengths that carry the most relevant information of the sensor, while accounting for contributions from harmonics and cross-talk, as depicted in Fig. 3.

Subsequently, we perform a scaling operation on the rows of matrix $\mathbf{H}$ to ensure that they sum to one. The sampled response matrix is

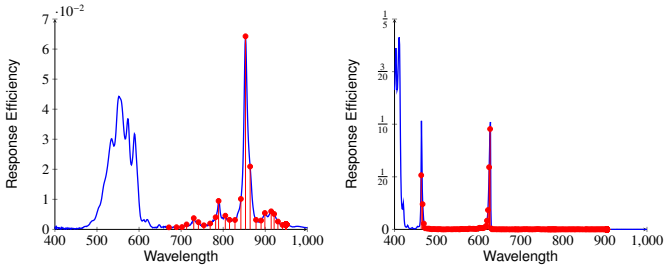

(a) Photonfocus SSI 5×5 [16] (b) Ximea linescan 192 bands [17]

Fig. 3. Fabry-Perot filter responses (in blue) for one band from linescan and SSI cameras with highlighted virtual wavelengths (in red)

denoted as $\mathbb{H}^{\mathbb{S}}$ and has dimensions $k \times m$, where m represents the number of virtual wavelengths. Thereafter, the size of the vector $\mathbf{x}$ is adjusted to $m \times 1$ and is referred to as $\mathbf{y}$ for clarity. To obtain $\mathbf{y}$, we aim to solve a nonnegative least-squares problem, i.e.,

$$\min_{\mathbf{y} \geq 0} \frac{1}{2} \|\mathbf{z} - \mathbb{H}^{\mathbb{S}} \cdot \mathbf{y}\|_2^2 + \frac{\alpha}{2} \cdot \|D \cdot \mathbf{y}\|_2^2 + \frac{\alpha}{2} \cdot \mathcal{R}(\mathbb{H}^{\mathbb{S}}, \mathbf{y}), \tag{4}$$

where $\mathcal{R}(\mathbb{H}^{\mathbb{S}}, \mathbf{y})$ is a regularization term defined as

$$\mathcal{R}(\mathbb{H}^{\mathbb{S}}, \mathbf{y}) = \|E(\mathbb{H}^{\mathbb{S}}) \cdot D \cdot \mathbf{y}\|_2^2, \tag{5}$$

where $E(\mathbb{H}^{\mathbb{S}})$ is diagonal matrix which accounts for the entropy of each column of the matrix $\mathbb{H}^{\mathbb{S}}$ as follows:

$$E(\mathbb{H}^{\mathbb{S}}) = \begin{cases} -\sum_{l=1}^{k} \mathbb{H}^{\mathbb{S}}_{l,j} \cdot \log(\mathbb{H}^{\mathbb{S}}_{l,j}) & \text{if } i = j, \\ 0 & \text{otherwise.} \end{cases} \tag{6}$$

Here, i and j are the row and column indices. The function $\mathcal{R}(\mathbb{H}^{\mathbb{S}}, \mathbf{y})$ particularly employes the entropy on the matrix $\mathbb{H}^{\mathbb{S}}$ and Tikhonov regularization on the vector $\mathbf{y}$, denoted as $D \cdot \mathbf{y}$. The latter is a square matrix that accounts for the discrete derivative of the spectrum $\mathbf{y}$.

The entropy is applied to each column of the matrix $\mathbb{H}^{\mathbb{S}}$ to automatically determine the degree of smoothness required in the estimation. In practice, it can be interpreted as follows: when the band response exhibits multiple peaks, the resulting matrix $\mathbb{H}^{\mathbb{S}}$ can be ill-conditioned, as most of its values will tend to be near zero. This situation results in a high entropy indicating a need for increased smoothness regularization. Conversely, when there is only a single peak, the entropy is zero, signifying that no additional penalization for smoothness is necessary. In summary, this method combines entropy regularization on the matrix $\mathbb{H}^{\mathbb{S}}$ and Tikhonov regularization on the vector $\mathbf{y}$, effectively balancing data fidelity and the desired level of smoothness in the estimated spectrum[1]. This approach ensures an adaptive optimization process for recovering $\mathbf{y}$, and we refer to it as "Scene-Dependent Spectral Correction" (SDS-Cor).

Finally, in the context of our proposed method, the possibility of doing super-resolution appears when considering scenarios without cut-off filters. In such cases, the full informational content of the harmonics in the response matrix $\mathbf{H}$ can be exploited for "super-spectral" resolution enhancement. This approach involves utilizing the extended range of harmonics data in matrix $\mathbf{H}$ to increase the spectral detail beyond the standard resolution. Our inverse problem

[1]Including the non-entropy-weighted regularization term $\|D \cdot \mathbf{y}\|_2^2$ ensures robustness in scenarios where entropy is zero. This case is rare, but this addition makes our method more general. Still, we found in preliminary tests that adding or removing this term does not significantly affect the achieved results.

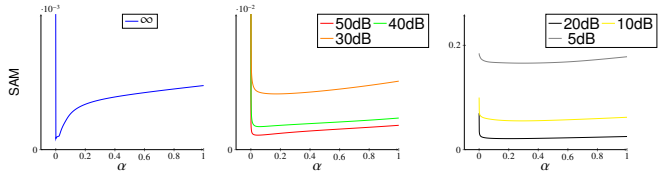

(a) Noiseless (b) 50, 40, and 30 dB (c) 20, 10, and 5 dB

Fig. 4. Reached SAM values vs the value of α and the input SNR.

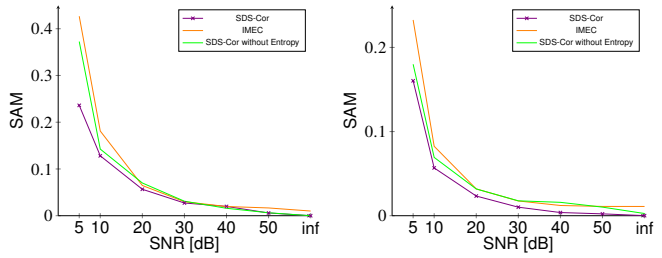

(a) Snapshot (b) Linescan

Fig. 5. Results on synthetic simulation used USGS spectral data

framework is well-suited to exploit this opportunity. By changing the dimensions of $\mathbf{H}$ and accordingly adjusting our spectral estimation process, we can effectively enhance the resolution of the spectral data. While this is not the core of the proposed paper, this point is also briefly investigated in the next section.

IV. EXPERIMENTS AND RESULTS

We conducted experiments to evaluate the effectiveness of our proposed method using synthetic simulations, and real images.

The synthetic experiment evaluated the spectral responses of water, metal, and concrete using spectral signatures from [18] and the response matrices of the Snapshot Mosaic [16] and Linescan Wedge cameras [17]. We simulated sensor responses to these materials, applied both our proposed and IMEC's correction methods [13], and assessed them by comparing the Spectral Angle Mapper (SAM) between corrected and original spectra under varying noise levels.

However, we first study the impact of the regularization parameter α on the NNLS problem. Fig. 4 shows how α affects the SAM value at different noise levels for the linescan camera. Optimal SAM values are obtained with $\alpha = 10^{-4}$ in noiseless scenarios, while higher noise requires larger α values to maintain deconvolution robustness. Throughout this study, $\alpha = 10^{-4}$ was used for noiseless synthetic experiments, with noise-specific optimal values determined from the plot. For the real data experiment, we set $\alpha = 0.0014$, assuming the cameras to generate images with an input SNR equal to 40 dB.

Our comparative analysis shown in Fig. 5, evaluates the performance across various noise levels and highlights the advantage of incorporating entropy weighting into SDS-Cor method. The comparison highlights SDS-Cor's superiority to the IMEC method in noisy and noise-free settings, showing greater fidelity to the original spectra even in high-noise conditions.

To further evaluate the effectiveness of our proposed method, we conducted experiments using a linescan camera [17]. The camera captured images of colored papers in red, green, and blue under natural sunlight. Subsequently, we measure the spectral information of the colored papers and the lemons using an ASD FieldSpec 4

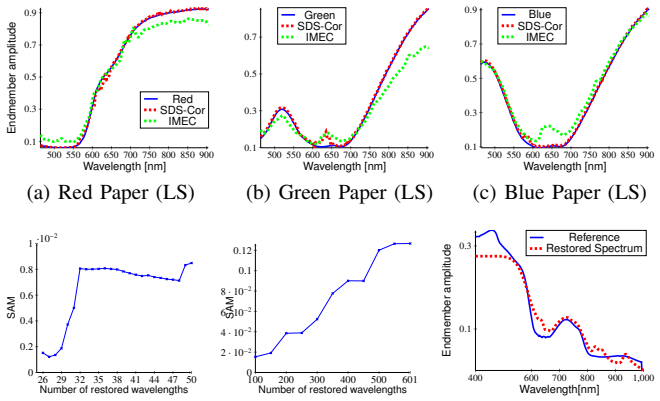

(a) Red Paper (LS) (b) Green Paper (LS) (c) Blue Paper (LS)

(d) Super-Resolution First Range (e) Super-Resolution Second Range (f) Water spectrum

Fig. 6. Spectral Correction and Analysis: Real Data and Super-Resolution Insights from Linescan (LS) and Snapshot (SSI) Cameras

spectrometer[2], serving as the reference dataset for our assessment. We then applied our method and IMEC correction matrix to the images and compared the corrected spectra with those obtained from the spectrometer measurements. Figs. 6(a), 6(b), and 6(c) display the restored spectra. Our proposed method outperforms the manufacturer solution with the linescan camera despite facing challenges in the spectral range between 600 and 700 nm, attributed to harmonics from the Fabry-Perot filters.

Finally, our proposed method can be used to enhance the resolution of hyperspectral imaging by performing super-resolution, starting directly from the response matrix of the sensor. The snapshot sensor [16] initially supported 25 distinct wavelengths within its active range. Our primary objective was to interpolate and restore additional spectral bands, mainly focusing on the midpoints between each pair of successive bands. For instance, given that the sensor supports bands at 650 nm and 680 nm, our first step was to accurately restore the band at 665 nm, which lies precisely in the middle of these two bands. This process was iteratively conducted for all available bands, gradually increasing the number of restored bands. As we progressed, the number of bands incrementally increased, reaching 49 bands. This enhancement effectively doubled the original spectral resolution of the sensor. To evaluate the effectiveness of this super-resolution process, we utilized the SAM for each stage of the reconstruction as the curve shows in Fig. 6(d). As the number of restored wavelengths increases, we observe a corresponding increase in the SAM angle, implying a reduction in the spectral reconstruction accuracy as shown in Fig. 6(e). Still, without any additional assumption, multiplying the spectral resolution by 24—i.e., expanding from 25 observed to 601 estimated bands—maintains a quite low SAM value (equal to 0.1). Fig. 6(f) shows the super-resolved spectrum of water in that case. These results highlight the relevance of the proposed work.

V. CONCLUSION AND DISCUSSION

In this work we introduced SDS-Cor, i.e., a novel approach developed to enhance spectral data correction in snapshot and linescan cameras. In contrast to the scene-independent spectral correction matrix provided by the manufacturer, our approach employs deconvolution techniques with entropy-weighted Tikhonov regularization to eliminate the generated impurities. By adapting to the specific attributes of the observed scene, SDS-Cor effectively removes harmonics and improves the quality of hyperspectral data. The experimental results on synthetic and real data demonstrated that the proposed method outperformed the manufacturer's solution even in the presence of noise. Our future work will focus on improving the method performance when the noise is introduced and expanding method's capabilities to address angularity correction simultaneously.

[2]See, e.g., https://www.malvernpanalytical.com/en/products/product-range/asd-range/fieldspec-range/fieldspec4-hi-res-high-resolution-spectroradiometer.

ACKNOWLEDGMENT

This work was partly funded by the Région Hauts-de-France and the Pôle Métropolitain de la Côte d'Opale. Experiments presented in this paper were carried out using the CALCULCO computing platform, supported by ULCO. Cameras used in the experiments were partly funded by ULCO and by FEDER within the HyperQSE project.

REFERENCES

[1] D. Manolakis, R. Lockwood, and T. Cooley, *Hyperspectral Imaging Remote Sensing: Physics, Sensors, and Algorithms*. Cambridge University Press, 2016.

[2] J. G. Michael West and C. Galvan, "Commercial snapshot spectral imaging: The art of the possible." Available online at https://www.mitre.org/sites/default/files/publications/pr-18-3832-commercial-snapshot-spectral-imaging-art-of-possible.pdf. Last access: 08/26/2022., 2018.

[3] B. Geelen, N. Tack, and A. Lambrechts, "A compact snapshot multispectral imager with a monolithically integrated per-pixel filter mosaic," in *Advanced Fabrication Technologies for Micro/Nano Optics and Photonics VII* (G. von Freymann, W. V. Schoenfeld, and R. C. Rumpf, eds.), SPIE, 2014.

[4] P. Chatelain, G. Delmaire, A. Alboody, M. Puigt, and G. Roussel, "Semi-automatic spectral image stitching for a compact hybrid linescan hyperspectral camera towards near field remote monitoring of potato crop leaves," *Sensors*, vol. 21, no. 22, 2021.

[5] N. Tack, A. Lambrechts, P. Soussan, and L. Haspeslagh, "A compact, high-speed, and low-cost hyperspectral imager," in *Silicon Photonics VII*, vol. 8266, p. 82660Q, International Society for Optics and Photonics, 2012.

[6] IMEC, "Hyperspectral sensors user manual." Available online at Support Portal of imec https://www.imec-int.com/, 2019.

[7] K. Vunckx and W. Charle, "Accurate video-rate multi-spectral imaging using imec snapshot sensors," in *Proc. IEEE WHISPERS'21*, pp. 1–7, 2021.

[8] K. Abbas, M. Puigt, G. Delmaire, and G. Roussel, "Locally-rank-one-based joint unmixing and demosaicing methods for snapshot spectral images. part ii: A filtering-based framework," *IEEE Trans. Comput. Imaging*, vol. 10, pp. 806–817, 2024.

[9] J. Zhang, R. Su, Q. Fu, W. Ren, F. Heide, and Y. Nie, "A survey on computational spectral reconstruction methods from rgb to hyperspectral imaging," *Scientific reports*, vol. 12, no. 1, p. 11905, 2022.

[10] T. Goossens, B. Geelen, J. Pichette, A. Lambrechts, and C. Van Hoof, "Finite aperture correction for spectral cameras with integrated thin-film Fabry–Perot filters," *Applied optics*, vol. 57, no. 26, pp. 7539–7549, 2018.

[11] J. Brauers and T. Aach, "A color filter array based multispectral camera," in *12. Workshop Farbbildverarbeitung* (G. C. Group, ed.), (Ilmenau), October 5-6 2006.

[12] K. Abbas, M. Puigt, G. Delmaire, and G. Roussel, "Joint unmixing and demosaicing methods for snapshot spectral images," in *Proc. IEEE ICASSP'23*, 2023.

[13] J. Pichette, T. Goossens, K. Vunckx, and A. Lambrechts, "Hyperspectral calibration method For CMOS-based hyperspectral sensors," in *Photonic Instrumentation Engineering IV* (Y. G. Soskind and C. Olson, eds.), vol. 10110, p. 101100H, International Society for Optics and Photonics, SPIE, 2017.

[14] T. Goossens, K. Vunckx, A. Lambrechts, and C. V. Hoof, "Spectral shift correction for fabry-perot based spectral cameras," in *Proc. IEEE WHISPERS*, 2019.

[15] J. Liu, S. Yuan, X. Zhu, Y. Huang, and Q. Zhao, "Nonnegative matrix factorization with entropy regularization for hyperspectral unmixing," *International Journal of Remote Sensing*, vol. 42, no. 16, pp. 6359–6390, 2021.

[16] Photonfocus, "Photonfocus snapshot mosaic camera cmv2k-sm5x5." https://www.photonfocus.com/products/camerafinder/camera/mv0-d2048x1088-c01-hs02-160-g2/, Last accessed: 2023-08-07.

[17] XIMEA, "Ximea - hyperspectral linescan usb3 camera 150 bands 470-900nm." https://www.ximea.com/en/products/hyperspectral-cameras-based-on-usb3-xispec/mq022hg-im-ls150-visnir, 2023.

[18] "U.S. Geological Survey (USGS) spectral library." https://www.usgs.gov/labs/spectroscopy-lab/science/spectral-library, Last accessed: 2022-10-24.